

AN IMPROVED IMAGE FILTERING METHOD BY USING WEIGHTED GUIDED IMAGE FILTER

K. SANDHYA¹, P.V.V.N.CHANAKYA²

¹PG Student, Dept. of ECE (DECS), NIET, Guntur, AP, India.

²Associate Professor, Dept. of ECE, NIET, Guntur, AP, India.

Abstract—It is known that local filtering-based edge preserving smoothing techniques suffer from halo artifacts. In this paper, a weighted guided image filter (WGIF) is introduced by incorporating an edge-aware weighting into an existing guided image filter (GIF) to address the problem. The WGIF inherits advantages of both global and local smoothing filters in the sense that: 1) the complexity of the WGIF is $O(N)$ for an image with N pixels, which is same as the GIF and 2) the WGIF can avoid halo artifacts like the existing global smoothing filters. The WGIF is applied for single image detail enhancement, single image haze removal, and fusion of differently exposed images. Experimental results show that the resultant algorithms produce images with better visual quality and at the same time halo artifacts can be reduced/avoided from appearing in the final images with negligible increment on running times.

Index Terms—Edge-preserving smoothing, weighted guided image filter, edge-aware weighting, detail enhancement, haze removal, exposure fusion.

I. INTRODUCTION

MOST application in computer vision and computer graphics engages image filtering to restrain and/or remove content in images. plain linear translation-invariant filters with explicit kernels, like mean, Gaussian, Laplacian, and Sobel filters, have been broadly used in image restoration, sharpening/blurring, feature extraction, edge detection etc. Alternatively, LTI filters be capable of implicitly performed by solving a Poisson Equation the same as in high dynamic range (HDR) compression, image matting, image stitching, and gradient domain manipulation. The filtering kernels

are absolutely described by means of the inverse of a homogenous Laplacian matrix. The LTI filtering kernels are spatially independent and invariant of image content. But usually one may desire to consider added information from a known guidance image. The prepare work of an isotropic distribution uses the incline of the filtering image itself to direct a diffusion process, steer clear of smoothing edges. The weighted least squares filter utilizes the filtering input (as an alternative of intermediate results, as in) as the guidance, and optimizes a quadratic function, which is the same to anisotropic diffusion with a nontrivial stable state. The guidance image is able to be another image besides the filtering input in several purposes. For illustration, in colorisation the chrominance channels be supposed to not bleed across luminance edges; in image matting the alpha not shiny should capture the thin structures in a combined image; in haze removal the depth layer should be consistent with the outlook. In these cases, we look upon the chrominance/alpha/depth layers as the image to be filtered, and the composite /luminance/scene as the guidance image, correspondingly. The filtering process is attained by optimizing a quadratic rate function weighted by the guidance image. The result is known by solving a large sparse matrix which only depends on the guide. This inhomogeneous matrix implicitly describes a translation-variant filtering kernel. While these optimization based approach frequently defer state-of-the-art class, it comes with the price of costly computational time. One more way to take benefit of the guidance image is to openly build it into filter kernels. The two-sided filter, independently wished-for in, and and later indiscriminate in, is perchance the most accepted one of like explicit filters. Its output at a pixel is a weighted average of the in close proximity pixels, where the weights depend on the color /intensity similarities in the guidance image. The guidance image itself can be the filter input or another image.

The two-sided filter can smooth small fluctuations and while preserving edges. However this filter is valuable in various states, it may have unnecessary gradient reversal artifacts near edges. The speedy execution of the bilateral filter is also a challenging problem. Latest techniques rely on quantization process to accelerate but may sacrifice accuracy. In this paper, we propose a novel precise image filter called guided filter. The filtering output is nearby a linear transform of the guidance image. On one side, the guided filter has fine edgepreserving smoothing property like the bilateral filter, but it does not experience from the gradient reversal artifacts. On the other side, the guided filter is capable of to be used beyond smoothing: With the help of the guidance image, it can create the filtering output more structured and less smoothed as compared to the input. We notice that the guided filter performs extremely well in a great range of applications, including image smoothing and enhancement, HDR firmness, flash-no-flash imaging, matting, feathering, dehazing, and joint up sampling. Moreover, the guided filter naturally has a time (in the number of pixels N) non -estimated algorithm for both high resolution images and gray-scale, regardless of the kernel size and intensity range. Classically, our CPU execution achieves 40 ms per mega-pixel executing grayscale filtering: To the best of our knowledge, this is one of the best edge preserving filters. A beginning description of this paper was published in ECCV '10. It is significance mentioning that the guided filter has witnessed a sequence of new applications since then. The guided filter allows a highquality real-time stereo matching algorithm. An alike stereo technique is proposed independently in the guided filter has also been applied in optical flow assessment, interactive image segmentation, saliency recognition, and illumination rendering. We accept as true that the guided filter has enormous potential in computer vision and graphics, given its ease, effectiveness, and high-quality. We have provided a public code to make easy future studies.

II. LITERATURE SURVEY

Zhengguo Li et. al. [1] —Weighted Guided Image Filtering! In this paper, It is identified that local filtering-based edge preserving smoothing method suffer from halo artifacts. In this paper, a weighted

guided image filter is initiated by incorporating an edge-aware weighting into an accessible guided image filter (GIF) to deal with the problem. The WGIF inherits benefit of both global and local smoothing filters in the sense that: 1) the difficulty of the WGIF is $O(N)$ for an image with N pixels, which is similar as the GIF and 2) the WGIF can keep away from halo artifacts like the present global smoothing filters. The WGIF is applied for single image detail improvement, single image haze deletion, and blend of differently exposed images. A weighted guided image filter is planned in this paper by incorporating an edgeaware weighting into the guided image filter .The WGIF preserves keen boundaries as well as presented global filters, and the difficulty of the WGIF is $O(N)$ for an image with N pixels which is almost same as GIF. Because of the simplicity of the WGIF, it has several applications in the field of computational photography and image processing. Mainly, it is useful to study single image aspect enhancement, fusion of differently exposed images, and single image haze removal. Investigational results illustrate that the resulting algorithms can produce images with excellent visual quality as those of global filters, and same time the running times of the planned algorithms are comparable to GIF based algorithms. Buyue Zhang et. al. [2] —Adaptive Bilateral Filter for Sharpness Enhancement and Noise Removall In this paper, we tend to present the adaptive bilateral filter (ABF) for sharpness improvement and noise removal. The ABF sharpen an representation by raise the incline of the edges while not manufacturing overshoot or undershoot. It's an approach to sharpness improvement that's basically different from the unsharp mask (USM). This new approach to slope restitution also differs significantly from previous slope restoration algorithms in this the ABF doesn't involve detection of edges or their direction, or pulling out of edge shape. In the ABF, the edge slope is enhanced by reworking the histogram through a variety of filter with adaptive offset and width. we tend to demonstrate that ABF works well for both natural pictures and text images. In this paper, we tend to there an adaptive bilateral filter (ABF). The ABF retains the general kind of the bilateral filter, but contains 2 necessary modifications. First, an offset is introduced to the range filter within the ABF. Second, both and also the width of the range filter in

the ABF are locally adaptive. They depend upon the local image structure, classified in line with the output of the Laplacian of Gaussian (LoG) operator applied to the degraded image. The optimal and are estimated in advance throughout the development of the algorithmic rule via an off-line training procedure employing a set of pairs of original and degraded images. During the training procedure, the MSE between the original and reconstructed images is reduced for each class of pixels. Anush Krishna Moorthy et. al. [3] —A Two-Step Framework for Constructing Blind Image Quality Indices| Now a day's No reference Image Quality Assessment (NR IQA) algorithms usually assume that the distortion affecting the picture is recognized. This is a preventive supposition for realistic applications; since in a majority of cases the distortions the picture are unidentified. We recommend a innovative 2-step framework for no-reference image quality assessment based on natural scene statistics (NSS). Previously trained, the frameworks don't require any knowledge of the distorting process and the framework is modular in that it can be extended to any number of distortions. We describe the framework for blind image quality consideration and a description of this framework—the blind image quality index (BIQI) is evaluated on the LIVE image quality assessment database. Jiahao Pang et. al. [4] —Improved Single Image Dehazing Using Guided Filter| Single image dehazing is challenging because it is massively ill-posed. Haze removal based on dark channel prior is effective, but refining the transmission map with closed-form matting is computationally expensive. Recent work discovered that using guided filter to refine the transmission map is feasible. In this paper, we intricate single image dehazing by combining dark channel prior and guided image filtering in detail. By analyzing the tradeoffs of this approach, we tend to propose an effective scheme to adapt the parameters Experiments and comparisons show that our method generates satisfactory dehazed results with low computation. In this paper, we elaborate single image dehazing by combining dark channel prior and guided image filtering, and then we study several aspects of this approach. Through experiments and analyses, we propose an effective scheme to adapt the patch size of dark channel and the filtering radius of guided filter. The main benefit of using guided filter to refine the transmission lies in

its low computational cost; it also generates comparable dehazed results with He et al.'s work. Since guided image filtering is an approximation of soft matting in, this method may fail when the input image contains abrupt depth changes. Fortunately, it turns out that our work performs quite well on many hazy images, its $O(N)$ time complexity also makes it appealing for many applications. Pierre Charbonnier et. al. [5] —Deterministic Edge-Preserving Regularization in Computed Imaging| Many image process problems are sick posed and must be regularised. Usually, a roughness penalty is imposed on the explanation. The complexity is to evade the smooth of edges, which are important attributes of the image. In this paper, we tend to 1st provide conditions for the design of such an edge-preserving regularization. Under these conditions, we tend to show that it's possible to introduce an auxiliary variable whose role is twofold. First, it marks the discontinuities and makes sure their perpetuation from flat. 2nd it makes the criterion halfquadratic. The optimisation is then easier. We tend to propose a deterministic strategy, based on alternate minimizations on the image and also the auxiliary variable. This results in the definition of an ingenious reconstruction algorithmic rule referred to as ARTUR. A number of theoretical property of ARTUR are discuss. Experimental results illustrate the behavior of the algorithmic rule. These results are shown in the field of tomography, but this technique can be applied in a large number of applications in image processing. In this document, we've measured the trouble of edge-preserving Regularization in computed imaging. Our first aim was to make available a united answer to the question, what belongings have to a possible work (or its derivative) satisfied to make sure the maintenance of edges. We've planned a heuristical study of the first-order necessary conditions which LED us to propose 3 conditions for edge preservation.

III. RELATED WORKS ON EDGE-PRESERVING SMOOTHING TECHNIQUES

In this section, existing edge-preserving smoothing techniques are summarized with the emphasis on the GIF in [14] and the WLS filter in [4]. The task of edge-preserving smoothing is to decompose an image X into two parts as follows:

$$X(p) = \hat{Z}(p) + e(p), \quad (1)$$

where \hat{Z} is a reconstructed image formed by homogeneous regions with sharp edges, e is noise or texture, and $p=(x, y)$ is a position. \hat{Z} and e are called base layer and detail layer, respectively. One type of edge-preserving smoothing techniques is based on local filtering. The BF is widely used due to its simplicity [9], [19],[20]. However, the BF could suffer from “gradient reversal” artifacts despite its popularity [14], and the results may exhibit undesired profiles around edges, usually observed in detail enhancement of conventional LDR images or tone mapping of HDR images. The GIF was introduced in [14] to overcome this problem. In the GIF, a guidance image G is used which could be identical to the image X to be filtered. It is assumed that \hat{Z} is a linear transform of G in the window $\Omega_{\zeta 1}(p)$ [21]–[23]:

$$\hat{Z}(p) = a_{p'}G(p) + b_{p'}, \quad \forall p \in \Omega_{\zeta 1}(p'), \quad (2)$$

where $\Omega_{\zeta 1}(p)$ is a square window centered at the pixel p of a radius $\Omega_{\zeta 1}$. $a_{p'}$ and $b_{p'}$ are two constants in the window $\Omega_{\zeta 1}(p')$. To determine the linear coefficients ($a_{p'}$, $b_{p'}$), a constraint is added to X and \hat{Z} as in Equation (1). The values of $a_{p'}$ and $b_{p'}$



Fig. 1. Two tone mapped images. (a) $\lambda = 2, \gamma = 1.2,$ and $\epsilon = 0.0001$ as in [4]; and (b) $\lambda = 2, \gamma = 0,$ and $\epsilon = 0$.

are then obtained by minimizing a cost function $E(a_{p'}, b_{p'})$ which is defined as

$$E = \sum_{p \in \Omega_{\zeta 1}(p')} [(a_{p'}G(p) + b_{p'} - X(p))^2 + \lambda a_{p'}^2], \quad (3)$$

where λ is a regularization parameter penalizing large $a_{p'}$. Besides the above local filtering based edge-preserving smoothing techniques, another type of edge-preserving smoothing techniques is based on

global optimization. The WLS filter in [4] is a typical example and it is derived by minimizing the following quadratic cost function:

$$E = \sum_{p=1}^N [(\hat{Z}(p) - X(p))^2 + \lambda(p)\|\nabla \hat{Z}(p)\|^2], \quad (4)$$

where N is the total number of pixels in an image, $\nabla \hat{Z}(p) = [\frac{\partial \hat{Z}(p)}{\partial x}, \frac{\partial \hat{Z}(p)}{\partial y}]^T$, and $\lambda(p) = [\lambda_x(p), \lambda_y(p)]^T$ is defined as

$$\lambda_x(p) = \frac{\lambda}{|\frac{\partial X(p)}{\partial x}|^\gamma + \epsilon}; \quad \lambda_y(p) = \frac{\lambda}{|\frac{\partial X(p)}{\partial y}|^\gamma + \epsilon},$$

λ, γ and ϵ are three constants. The values of λ, γ and ϵ in [4] are 2, 1.2 and 10⁻⁴, respectively. It is shown in the linear model (2) that $\nabla \hat{Z}(p) = a_{p'} \nabla G(p)$. Clearly, the smoothness of \hat{Z} in $\zeta 1(p)$ depends on the value of $a_{p'}$. This implies that the data term and the regularization terms in the GIF are similar to those in the WLS filter in the sense that the data term measures the fidelity of \hat{Z} with respect to the filtered image X and the regularization term provides the smoothness level of \hat{Z} . There are two major differences between the WLS filter and the GIF. 1) The GIF in [14] is based on local optimization while the WLS filter in [4] on global optimization. As such, the complexity of the GIF is $O(N)$ for an image with N number of pixels and the WLS filter is more complicated than the GIF. 2) The value of λ is fixed in the GIF while it is adaptive to local gradients in the WLS filter. One possible problem for the GIF is halos which can be avoided by the WLS filter. As indicated in [14], the GIF would concentrate blurring near edges and introduce halos while the WLS filter would distribute the blurring globally. Here, we would argue that the latter is another possibly major reason that halo artifacts can be avoided by the WLS filter. To support our argument, the WLS filter is applied to design a tone mapping algorithm for HDR images. Two tone mapped images are shown in Fig. 1. With the values of λ, γ and ϵ in [4], halo artifacts are avoided from appearing in the final



Fig. 2. (a) An input image, and (b) its weighting.

tone mapped image. However, halo artifacts appear in the final image when the values of $\lambda_x(p)$ and $\lambda_y(p)$ are fixed as λ_s . This implies that the spatially varying image gradients aware weighting $\lambda_x(p)$ and $\lambda_y(p)$ are crucial for the WLS filter in [4] to avoid halo artifacts. Unfortunately, the value of λ in the GIF [14] is fixed rather than being spatially varying as in [4]. As such, halos are unavoidable for the GIF in [14] when it is forced to smooth edges.

IV. WEIGHTED GUIDED IMAGE FILTER

In this section, an edge-aware weighting is first proposed and it is incorporated into the GIF in [14] to form the WGIF.

A. An Edge-Aware Weighting

Let G be a guidance image and $\sigma_{G,1}^2(p)$ be the variance of G in the 3×3 window, $1(p)$. An edge-aware weighting $\Gamma_G(p)$ is defined by using local variances of 3×3 windows of all pixels as follows:

$$\Gamma_G(p') = \frac{1}{N} \sum_{p=1}^N \frac{\sigma_{G,1}^2(p') + \epsilon}{\sigma_{G,1}^2(p) + \epsilon}, \quad (5)$$

where ϵ is a small constant and its value is selected as $(0.001 \times L)^2$ while L is the dynamic range of the input image. All pixels in the guidance image are used in the computation of $\Gamma_G(p')$. In addition, the weighting $\Gamma_G(p)$ measures the importance of pixel p with respect to the whole guidance image. Due to the box filter in [14], the complexity of $\Gamma_G(p')$ is $O(N)$ for an image with N pixels. The value of $\Gamma_G(p')$ is usually larger than 1 if p is at an edge and smaller than 1 if p is in a smooth area. Clearly, larger weights are assigned to pixels at edges than those pixels in flat areas by using the weight $\Gamma_G(p')$ in Equation (5). Applying this edge-aware weighting,

there might be blocking artifacts in final images. To prevent possible blocking artifacts from appearing in the final image, the value of $\Gamma_G(p')$ is smoothed by a Gaussian filter. The smoothed weights of all pixels in Fig. 2(a) are shown in Fig. 2(b). Clearly, larger weights are assigned to pixels at edges than those pixels in flat areas. The proposed weighting matches one feature of human visual system, i.e., pixels at sharp edges are usually more important than those in flat areas [17]. It should be pointed out that the proposed weighting $\Gamma_G(p')$ is one edge-aware weighting, and there are many other edge-aware weighting including those derived by the

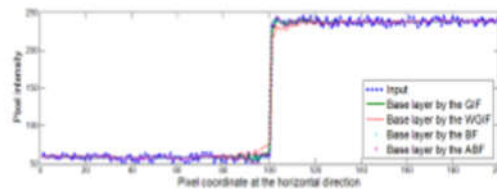


Fig. 3. 1-D illustration of the WGIF, the GIF in [14], the BF in [9], and the ABF in [16]. The values of ζ_1 and λ in both the WGIF and the GIF are 15 and 1/64, respectively. The values of σ_1 and σ_2 in both the BF and the ABF are 15 and 0.2, respectively.

Sobel gradient and the Roberts gradient [24]. The GIF can be improved by incorporating these edge-aware weighting into the GIF. In the following section, the proposed weighting $\Gamma_G(p')$ in Equation (5) is used as an example to illustrate the WGIF.

B. The Proposed Filter

Same as the GIF, the key assumption of the WGIF is a local linear model between the guidance image G and the filtering output \hat{Z} as in Equation (2). The model ensures that the output \hat{Z} has an edge only if the guidance image G has an edge. The proposed weighting $\Gamma_G(p')$ in Equation (5) is incorporated into the cost function $E(ap', bp')$ in Equation (3). As such, the solution is obtained by minimizing the difference between the image to be filtered X and the filtering output \hat{Z} while maintaining the linear model (2), i.e., by minimizing a cost function $E(ap', bp')$ which is defined as

$$E = \sum_{p \in \Omega_{\zeta_1}(p')} [(a_{p'}G(p) + b_{p'} - X(p))^2 + \frac{\lambda}{\Gamma_G(p')} a_{p'}^2] \quad (6)$$

The optimal values of $a_{p'}$ and $b_{p'}$ are computed as

$$a_{p'} = \frac{\mu_{G \odot X, \zeta_1}(p') - \mu_{G, \zeta_1}(p') \mu_{X, \zeta_1}(p')}{\sigma_{G, \zeta_1}^2(p') + \frac{\lambda}{\Gamma_G(p')}} \quad (7)$$

$$b_{p'} = \mu_{X, \zeta_1}(p') - a_{p'} \mu_{G, \zeta_1}(p') \quad (8)$$

where \odot is the element-by-element product of two matrices. $\mu_{G \odot X, \zeta_1}(p')$, $\mu_{G, \zeta_1}(p')$ and $\mu_{X, \zeta_1}(p')$ are the mean values of $G \odot X$, G and X , respectively.

The final value of $\hat{Z}(p)$ is given as follows:

$$\hat{Z}(p) = \bar{a}_p G(p) + \bar{b}_p \quad (9)$$

where \bar{a}_p and \bar{b}_p are the mean values of $a_{p'}$ and $b_{p'}$ in the window computed as

$$\bar{a}_p = \frac{1}{|\Omega_{\zeta_1}(p)|} \sum_{p' \in \Omega_{\zeta_1}(p)} a_{p'}; \quad \bar{b}_p = \frac{1}{|\Omega_{\zeta_1}(p)|} \sum_{p' \in \Omega_{\zeta_1}(p)} b_{p'} \quad (10)$$

and $|\Omega_{\zeta_1}(p)|$ is the cardinality of $\Omega_{\zeta_1}(p)$. For easy analysis, the images X and G are assumed to be the same. Consider the case that the pixel p is at an edge. The value of $\Gamma_G(p')$ is usually much larger than 1. $a_{p'}$ in the WGIF is closer to 1 than $a_{p'}$ in the GIF [14]. This implies that sharp edges are preserved better by the WGIF than the GIF. As shown in Fig. 3, edges are indeed preserved much better

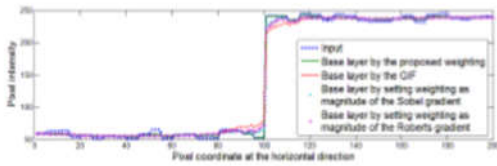


Fig. 4. 1-D illustration of three different WGIFs and the GIF in [14]. The values of ζ_1 and λ are 15 and 1/32, respectively.

by the WGIF. In addition, the complexity of the WGIF is $O(N)$ for an image with N pixels which is the same as that of the GIF. Edges are also preserved well by the ABF in [16] while the complexity of the ABF is an issue.

V. APPLICATIONS OF THE WGIF

In this section, the WGIF is adopted to study single image detail enhancement, single image haze removal, and fusion of differently exposed images. All algorithms are implemented by using the MATLAB 2008b, and all the simulations were carried on Dell Precision T7400 with Intel Quad Core CPU 3.2 GHz and 4GB of RAM. Readers are invited to view the electronic version of the full-size figures

in order to better appreciate the differences among images

A) Single Image Detail Enhancement:

We first consider the case that the whole image is enhanced and it is called “full detail enhancement”. With the WGIF, the input image X is decomposed into \hat{Z} and e as shown in Equation (1) and the details enhancement can be achieved as follows:

$$Z_{\text{enh}}(p) = X(p) + \theta e(p) \quad (11)$$

where $\theta (> 0)$ is a positive constant and is called an amplification factor.

Since this paper focuses on introducing an edge-aware weighting to the GIF, three different methods on the computation of edge-aware weighting are first compared, and one is the proposed weighting in Equation (5) and the other two are

$$\hat{\Gamma}_G(p') = \sqrt{\left(\frac{\partial Z(p')}{\partial x}\right)_s^2 + \left(\frac{\partial Z(p')}{\partial y}\right)_s^2} \quad (12)$$

$$\check{\Gamma}_G(p') = \sqrt{\left(\frac{\partial Z(p')}{\partial x}\right)_r^2 + \left(\frac{\partial Z(p')}{\partial y}\right)_r^2} \quad (13)$$

$\hat{\Gamma}_G(p')$ is the magnitude of the Sobel gradient, and $\check{\Gamma}_G(p')$ is the magnitude of the Roberts gradient. Similar to Fig. 3, a simple 1-D example is tested.

It is illustrated in Fig. 4 that the proposed weighting preserves edges slightly better than both $\hat{\Gamma}_G(p')$ and $\check{\Gamma}_G(p')$

Besides comparing three different methods on the computation of weighting, the WGIF is compared with the GIF by choosing three different values of θ as 1, 4 and 9. The quality metric is used to evaluate enhanced images. The scores of the six images in Fig. 5 are 37.84, 40.98, 38.37, 55.97, 35.89, and 57.89,

respectively. With the metric, a higher value represents a higher quality. It is also shown in Fig. 5

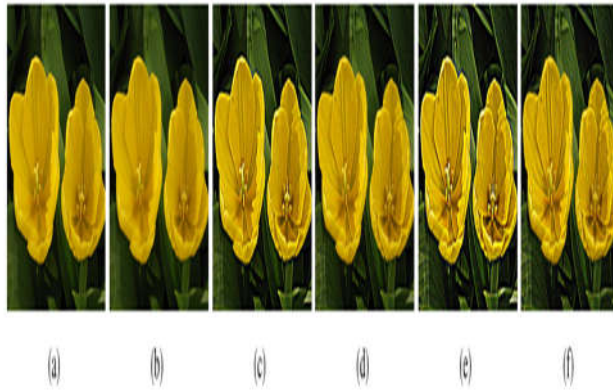


Fig5: Comparison of the WGIF with the GIF in [14] by choosing four different values of θ . The values of ζ_1 and λ are 15 and 1/128, respectively. (a, c, e) by the GIF in [14] with the value of θ as 1, 4, and 9, respectively, (b, d, f) by the WGIF with the value of θ as 1, 4, and 9, respectively

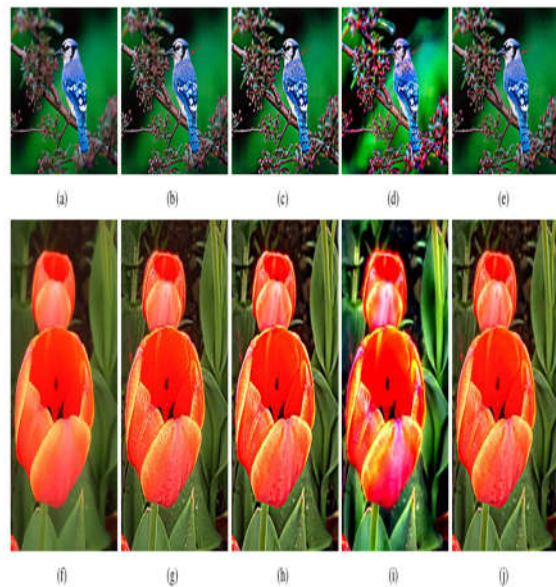


Fig 6: Comparison of enhanced images via different filters. (a, f) images to be enhanced, (b, g) enhanced image by the BF in [9], (c, h) enhanced images by the GIF in [14], (d, i) enhanced images by the global filter in [8], (e, j) enhanced images by the WGIF.

that the GIF in is more sensitive to the value of θ in terms of halo artifacts. The halo artifacts by the GIF as well as the amplified noise by both the GIF and the WGIF become more visible when the value of θ is enlarged. This implies that the value of θ also plays an important role in the generation of halo artifacts and the amplification of noise. The observation will serve as a guideline for the design of single image haze removal algorithm.

Two images are also tested to compare the WGIF with the BF, the GIF and the l0 norm based global optimization algorithm. The values of σ_1 and σ_2 are 16 and 0.1 for the BF. The values of λ and ζ_1 are respectively selected as 1/128 and 16 for both the WGIF and the GIF. κ and λ are respectively set as 2 and 0.02 as in the MATLAB code provided by the authors. As indicated by the red arrows in Fig. 6, the WGIF can be used to produce enhanced images with better visual quality. In addition, halo artifacts are avoided via the WGIF while there are halo artifacts in output images by the GIF and the BF, and gradient reversal artifacts by the global optimization based algorithm. The quality metric is also used to evaluate the enhanced images. As shown in Table 1, the objective quality is also improved by the WGIF.

The proposed detail enhancement algorithm in Equation (11) and the existing ones amplify all fine details of an input image to obtain an image with more fine details. However, there is a fundamental limitation for full detail enhancement algorithms, i.e., noise is also amplified when fine details are enhanced. The human visual system can tolerate amplified noise in complex regions but is particularly sensitive to amplified noise in flat areas. Separating the noise from fine details is also known to be very challenging. To overcome the limitation of full detail enhancement algorithms, a selective detail enhancement algorithm is introduced as follows:

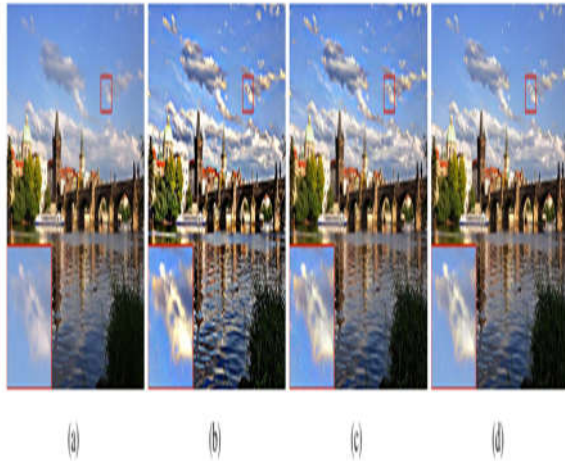


Fig 7: Comparison of full and selective detail enhancement algorithms. (a) an image to be enhanced, (b) an amplified image by the full detail enhancement algorithm based on the GIF in [14], (c) an amplified image by the full detail enhancement algorithm in Equation (11), (d) an amplified image by the selective detail enhancement algorithm in Equation (14).

where the value of $\eta(p)$ is computed by using $G(p)$ in Equation (5).

Its value is almost 0 if the pixel p is in a flat region and 1 otherwise

TABLE 1

Objective Evaluation On The Enhanced Images In Fig. 6

Image	1	2	3	4	5
Top	27.22	27.34	27.81	28.52	37.7
Bottom	36.8	48.5	33.0	41.7	35.9
m	7	7	4	2	1

B)Single Image Haze Removal:

Images of outdoor scenes could be degraded by haze, fog, and smoke in the atmosphere. The degraded images lose the contrast and color fidelity. Haze removal is thus highly desired in both computational photography and computer vision applications. The model adopted to describe the formulation of a haze image is given as

$$X_c(p) = \hat{Z}_c(p)t(p) + A_c(1 - t(p)) \quad (15)$$

When the atmosphere is homogenous, the transmission $t(p)$ can be expressed as:

$$t(p) = e^{-ad(p)} \quad (16)$$

Let $\phi_c(\cdot)$ be a minimal operation along the color channel $\{r, g, b\}$ and it is defined as

$$A_{\min} = \phi_c(A_c) = \min\{A_r, A_g, A_b\} \quad (17)$$

$$X_{\min}(p) = \phi_c(X_c(p)) = \min\{X_r(p), X_g(p), X_b(p)\} \quad (18)$$

$$\hat{Z}_{\min}(p) = \phi_c(\hat{Z}_c(p)) = \min\{\hat{Z}_r(p), \hat{Z}_g(p), \hat{Z}_b(p)\} \quad (19)$$

it can be derived from the haze image model in Equation (15) that

$$X_{\min}(p) = \hat{Z}_{\min}(p)t(p) + A_{\min}(1 - t(p)) \quad (20)$$

Let $\psi_{\zeta_2}(\cdot)$ be a minimal operation in the neighborhood $\psi_{\zeta_2}(p)$ and it is defined as

$$\psi_{\zeta_2}(z(p)) = \min_{p' \in \Omega_{\zeta_2}(p)} \{z(p')\} \quad (21)$$

It is shown that the complexity of $\psi_{\zeta_2}(\cdot)$ is $O(N)$ for an image with N pixels. The dark channel is defined as

$$J_{\text{dark}}^z(p) = \phi_c(\psi_{\zeta_2}(\hat{Z}_c(p))) \quad (22)$$

where the value of ζ_2 is 7. Even though the complexity of $\psi_{\zeta_2}(\cdot)$ is $O(N)$ for an image with N pixels, three minimal operations $\psi_{\zeta_2}(\cdot)$ and one minimal operation $\phi_c(\cdot)$ are required to compute $J_{\text{dark}}^z(p)$ for the pixel p . simplified dark channel is defined as

$$\hat{J}_{\text{dark}}^z(p) = \psi_{\zeta_2}(\phi_c(\hat{Z}_c(p))) \quad (23)$$

The value of $t(p)$ is assumed to be constant in the neighborhood $\Omega_{\zeta_1}(p')$. It can be derived from Equation (20) that

$$\hat{\mathbf{J}}_{\text{dark}}^{\mathbf{x}}(\mathbf{p}) = \hat{\mathbf{J}}_{\text{dark}}^{\mathbf{z}}(\mathbf{p}) \mathbf{t}(\mathbf{p}) + \mathbf{A}_{\text{min}}(\mathbf{1} - \mathbf{t}(\mathbf{p})) \quad (24)$$

Since $\hat{\mathbf{J}}_{\text{dark}}^{\mathbf{z}}(\mathbf{p}) \approx 0$, the value of $\mathbf{t}(\mathbf{p})$ can be initially estimated as

$$\mathbf{t}(\mathbf{p}) = \mathbf{1} - \frac{\hat{\mathbf{J}}_{\text{dark}}^{\mathbf{x}}(\mathbf{p})}{\mathbf{A}_{\text{min}}} \quad (25)$$

It is worth noting that the initial value of $\mathbf{t}(\mathbf{p})$ is given as

$$\mathbf{t}(\mathbf{p}) = \mathbf{1} - \Phi_c \left(\Psi_{\zeta_2} \left(\frac{\hat{\mathbf{Z}}_c(\mathbf{p})}{\mathbf{A}_c} \right) \right) \quad (26)$$

The initial value of $\mathbf{t}(\mathbf{p})$ is then computed as

$$\mathbf{t}(\mathbf{p}) = \mathbf{1} - \frac{31}{32} \frac{\hat{\mathbf{J}}_{\text{dark}}^{\mathbf{x}}(\mathbf{p})}{\mathbf{A}_{\text{min}}} \quad (27)$$

The value of λ is set to 1/1000 and the value of ζ_1 to 60. The value of the transmission map $\mathbf{t}(\mathbf{p})$ is further adjusted as

$$\mathbf{t}(\mathbf{p}) = \mathbf{t}^{1+\zeta}(\mathbf{p}) \quad (28)$$

where the value of ζ is adaptive to the haze level of the input image. Its value is 0/0.03125/0.0625 if the input image is with light/normal/heavy haze.

Finally, the scene radiance $\hat{\mathbf{Z}}(\mathbf{p})$ is recovered by

$$\hat{\mathbf{Z}}_c(\mathbf{p}) = \frac{X_c(\mathbf{p}) - A_c}{\mathbf{t}(\mathbf{p})} + A_c; \mathbf{c} \in \{r, g, b\} \quad (29)$$

Equation (29) is equivalent to

$$\begin{aligned} \hat{\mathbf{Z}}_c(\mathbf{p}) &= \mathbf{X}_c(\mathbf{p}) \\ &+ \left(\frac{1}{\mathbf{t}(\mathbf{p})} - 1 \right) (\mathbf{X}_c(\mathbf{p}) - \mathbf{A}_c) \end{aligned} \quad (30)$$

Since the color of the sky is usually very similar to the atmospheric light A_c in a haze image, it can be shown that

$$\frac{\hat{\mathbf{J}}_{\text{dark}}^{\mathbf{x}}(\mathbf{p})}{\mathbf{A}_{\text{min}}} \rightarrow \mathbf{1}, \text{ and, } \frac{1}{\mathbf{t}(\mathbf{p})} - 1 \rightarrow 31 \quad (31)$$

C) Fusion of Differently Exposed Images:

One of the challenges in digital image processing research is the rendering of a HDR natural scene on a conventional LDR display. This challenge can be addressed by capturing multiple LDR images at different exposure levels. Each LDR image only records a small portion of the dynamic range and partial scene details but the whole set of LDR images collectively contain all scene details.

All the differently exposed images can be fused together to produce a LDR image by an exposure fusion algorithm. Similar to the detail enhancement of a LDR image, halo artifacts, gradient reversal artifacts and amplification of noise in smooth regions are three major problems to be addressed for the fusion of differently exposed images. The overall local variance at pixel \mathbf{p} is thus computed as

$$\begin{aligned} \bar{\sigma}^2(\mathbf{p}') &= \frac{\sum_{k=1}^L \mathbf{w}_k(\mathbf{p}') (\sigma_{\log(y_k),1}^2(\mathbf{p}') + 0.001)}{\sum_{k=1}^L \mathbf{w}_k(\mathbf{p}')} \end{aligned} \quad (32)$$

Where $\mathbf{w}_k(\mathbf{p}')$ is given as

$$\begin{aligned} \mathbf{w}_k(\mathbf{p}') &= 77\gamma(\mathbf{z}_{k,1}(\mathbf{p}')) + 150\gamma(\mathbf{z}_{k,2}(\mathbf{p}')) + 29\gamma(\mathbf{z}_{k,3}(\mathbf{p}')) \\ \gamma(\mathbf{z}) &= \begin{cases} \mathbf{z} + 1; & \text{if } \mathbf{z} \leq 256 \\ 256 - \mathbf{z}; & \text{otherwise} \end{cases} \end{aligned} \quad (33)$$

And the weighted function is defined as

The value of $\Gamma_c(\mathbf{p}')$ is then given as

$$\Gamma_G(\mathbf{p}') = \frac{1}{N} \sum_{p=1}^N \frac{\bar{\sigma}^2(\mathbf{p}')}{\bar{\sigma}^2(\mathbf{p}')} \quad (34)$$

All the extracted fine details $L_k^{(d)}$ are fused by considering the exposedness levels of all image to produce the final fine details as

$$\mathbf{L}^{(d)}(\mathbf{p}) = \frac{\sum_{k=1}^L L_k^{(d)}(\mathbf{p}) \mathbf{w}_k(\mathbf{p})}{\sum_{k=1}^L \mathbf{w}_k(\mathbf{p})} \quad (35)$$

The final image is produced as

$$\mathbf{X}_f(\mathbf{p}) = \mathbf{X}_{\text{int}}(\mathbf{p}) e^{\mathbf{L}^{(d)}(\mathbf{p})} \quad (36)$$

Therefore, the WGIF can be applied to design a detail enhanced fusion algorithm with the fast speed of the

GIF based algorithm and at the same time, it has excellent visual quality of the global optimization based algorithm.

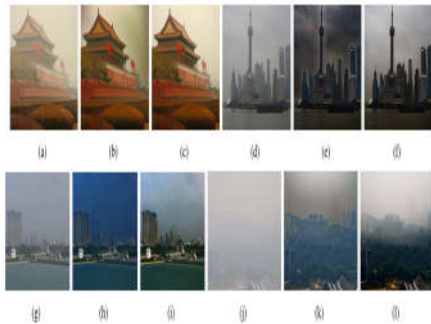


Fig 8: Comparison of the proposed haze removal algorithm and the haze removal algorithm in [14]. (a, d, g, j) four images with haze; (b, e, h, k) de-hazed images by the algorithm in [14]; (c, f, i, l) de-hazed images by the proposed algorithm.

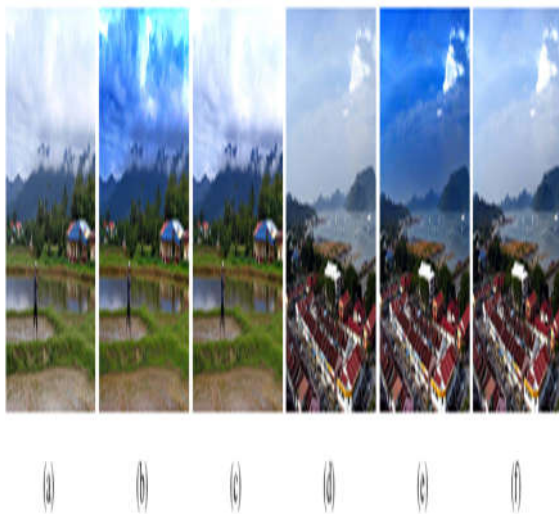


Fig 9: Comparison of the proposed haze removal algorithm and the haze removal algorithm in [14] by using two sets of images without haze. (a, d) two images without haze; (b, e) de-hazed images by the algorithm in [14]; (c, f) de-hazed images by the proposed algorithm.

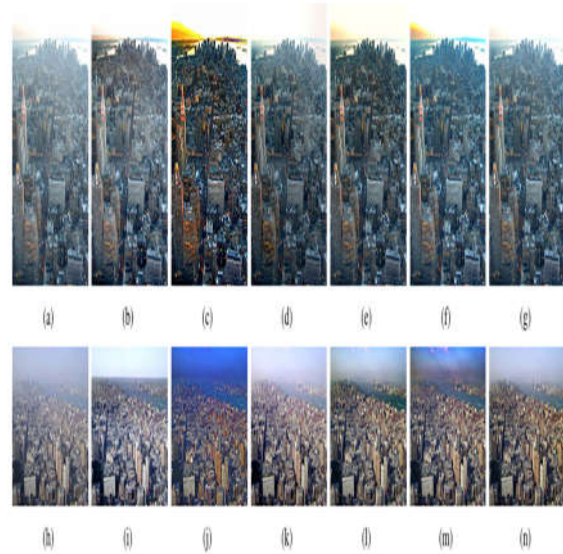


Fig 10: Haze removal results by the algorithms in [7], [14], [27], [33], and [34] and the proposed algorithm. (a, h) input images; (b, i) de-hazed images by the algorithm in [34]; (c, j) de-hazed images by the algorithm in [27]; (d, k) de-hazed images by the algorithm in [33]; (e, l) de-hazed images by the algorithm in [7]; (f, m) de-hazed images by the algorithm in [14]; and (g, n) de-hazed images by the proposed algorithm.

VI. RESULTS

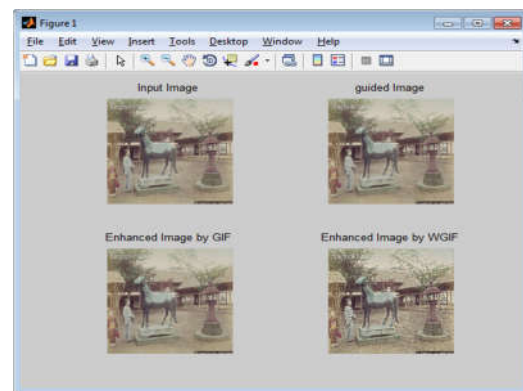


Figure 11: (a) Input image (b) Guided image (c) Enhanced image by GIF (d) Enhanced image by WGIF

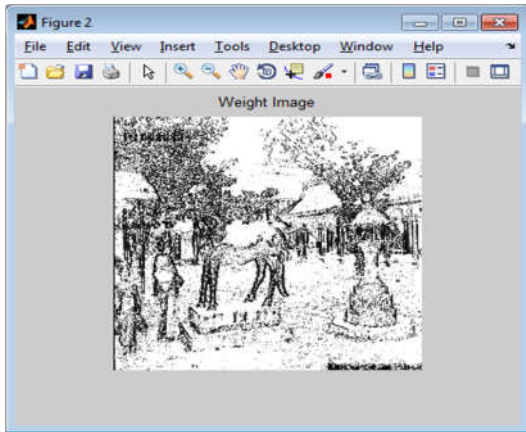


Figure 12: Weighted image

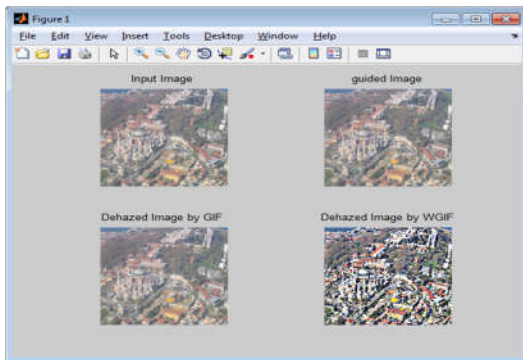


Figure 13: (a) Input image (b) Guided image (c) Dehazed image by GIF (d) Dehazed image by WGIF

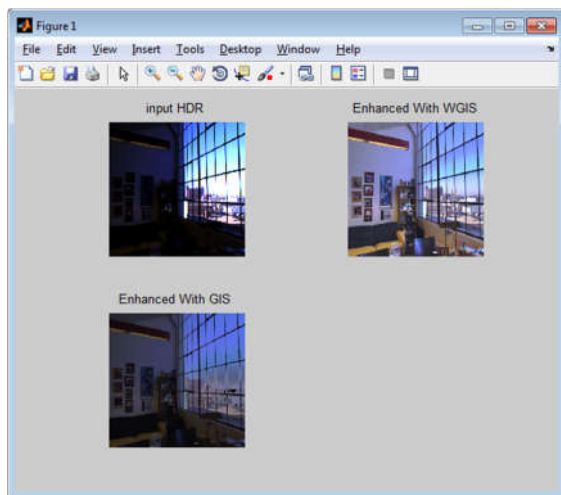


Figure 14: (a) Input HDR (b) Enhanced with WGIS (c) Enhanced with GIS

EXTENSION:

The extension work is performed on videos, where this video consists of no. of frames. Each frame is converted into image, because filtering on frame is impossible due to its change of pixel rate. Each image is filtered by WGIF technique to avoid halo artifacts and to reduce the complexity. After then each image is again converted into frame and then video. The improved quality of video is shown in below results.

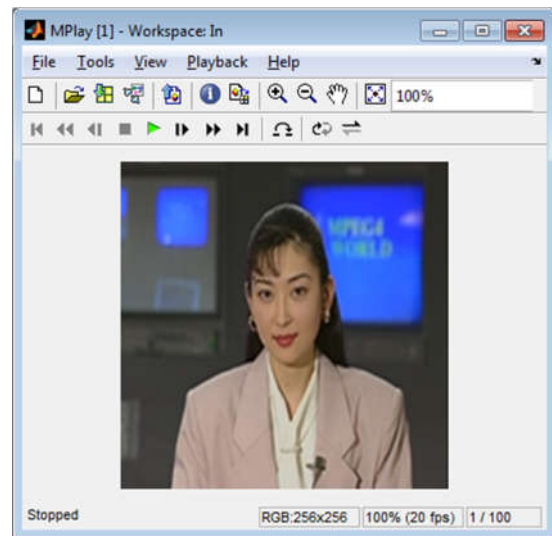


Figure 15: Input video

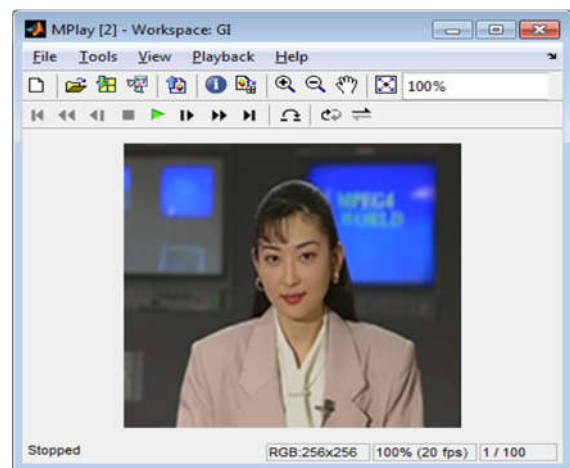


Figure 16: Guided approach for videos

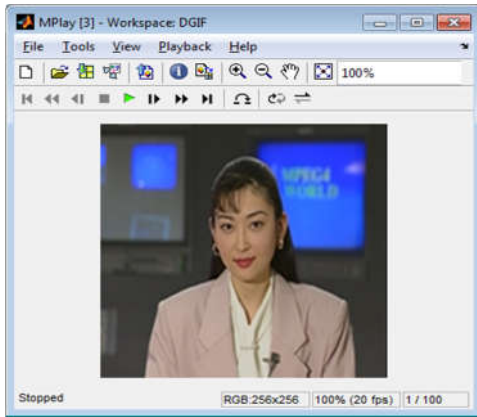


Figure 17: Guided image filtering approach for videos

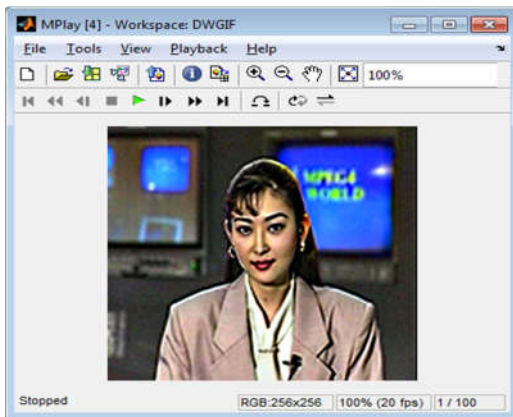


Figure 18: Weighted Guided image filtering approach for videos

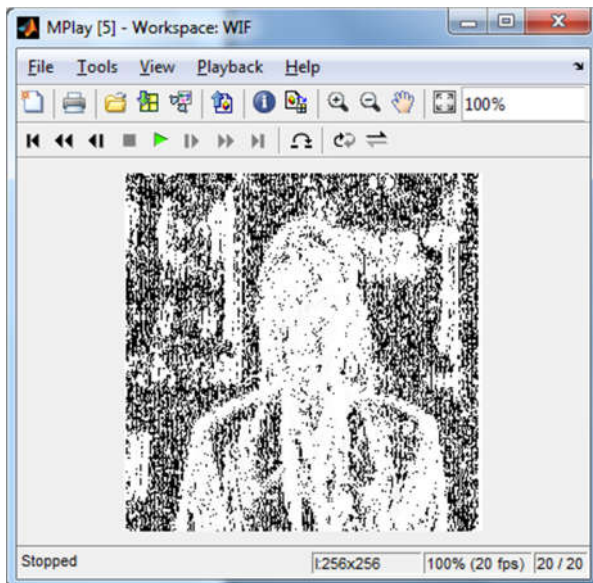


Figure 19: Applying weights for videos

VII.CONCLUSION

This method is introduced by incorporating an edge-aware weighted into an existing guided image filter (GIF). It has two advantages of both global and local smoothing filter in the sense-

- (1) Its complexity is 0,
- (2) Avoid halo artifacts

The output of WGIF results in better visual quality and avoid halo artifacts. , it has many applications in the fields of computational photography and image processing. Particularly, it is applied to study single image detail enhancement, single image haze removal, and fusion of differently exposed images.

Experimental results show that the resultant algorithms can produce images with excellent visual quality as those of global filters, and at the same time the running times of the proposed algorithms are comparable to the GIF based algorithms.

It is noting that the WGIF can also be adopted to design a fast local tone mapping algorithm for high dynamic range images, joint up sampling, flash/no-flash de-noising, and etc.

In addition, similar idea can be used to improve the anisotropic diffusion , Poisson image editing, etc. All these research problems will be studied in our future research.

Weighted guided filtering for image fusion gives efficient visual quality fused image. As specifies the weightage to pixels ,edges can be well preserved. It can be implemented in MATLAB and can produce the desired output. .

It has many applications in the fields of photography and image processing due to the simple attitude of the WGIF. Single picture fusion of differently exposed images, detail enhancement, haze removal, and it is applied.

The algorithms can make to produce images with excellent visual quality as those of global filters. Comparable to the GIF based algorithms the running time.

REFERENCES

- [1] P. Charbonnier, L. Blanc-Feraud, G. Aubert, and M. Barlaud, "Deterministic edge-preserving regularization in computed imaging," *IEEE Trans. Image Process.*, vol. 6, no. 2, pp. 298–311, Feb. 1997.
- [2] L. I. Rudin, S. Osher, and E. Fatemi, "Nonlinear total variation based noise removal algorithms," *Phys. D, Nonlinear Phenomena*, vol. 60, nos. 1–4, pp. 259–268, Nov. 1992.
- [3] Z. G. Li, J. H. Zheng, and S. Rahardja, "Detail-enhanced exposure fusion," *IEEE Trans. Image Process.*, vol. 21, no. 11, pp. 4672–4676, Nov. 2012.
- [4] Z. Farbman, R. Fattal, D. Lischinski, and R. Szeliski, "Edge-preserving decompositions for multi-scale tone and detail manipulation," *ACM Trans. Graph.*, vol. 27, no. 3, pp. 249–256, Aug. 2008.
- [5] R. Fattal, M. Agrawala, and S. Rusinkiewicz, "Multiscale shape and detail enhancement from multi-light image collections," *ACM Trans. Graph.*, vol. 26, no. 3, pp. 51:1–51:10, Aug. 2007.
- [6] P. Pérez, M. Gangnet, and A. Blake, "Poisson image editing," *ACM Trans. Graph.*, vol. 22, no. 3, pp. 313–318, Aug. 2003.
- [7] K. He, J. Sun, and X. Tang, "Single image haze removal using dark channel prior," *IEEE Trans. Pattern Anal. Mach. Intell.*, vol. 33, no. 12, pp. 2341–2353, Dec. 2011.
- [8] L. Xu, C. W. Lu, Y. Xu, and J. Jia, "Image smoothing via L0 gradient minimization," *ACM Trans. Graph.*, vol. 30, no. 6, Dec. 2011, Art. ID 174.
- [9] C. Tomasi and R. Manduchi, "Bilateral filtering for gray and color images," in *Proc. IEEE Int. Conf. Comput. Vis.*, Jan. 1998, pp. 836–846.
- [10] Z. Li, J. Zheng, Z. Zhu, S. Wu, and S. Rahardja, "A bilateral filter in gradient domain," in *Proc. Int. Conf. Acoust., Speech Signal Process.*, Mar. 2012, pp. 1113–1116.
- [11] P. Choudhury and J. Tumblin, "The trilateral filter for high contrast images and meshes," in *Proc. Eurograph. Symp. Rendering*, pp. 186–196, 2003.
- [12] F. Durand and J. Dorsey, "Fast bilateral filtering for the display of highdynamic-range images," *ACM Trans. Graph.*, vol. 21, no. 3, pp. 257–266, Aug. 2002.
- [13] J. Chen, S. Paris, and F. Durand, "Real-time edge-aware image processing with the bilateral grid," *ACM Trans. Graph.*, vol. 26, no. 3, pp. 103–111, Aug. 2007.
- [14] K. He, J. Sun, and X. Tang, "Guided image filtering," *IEEE Trans. Pattern Anal. Mach. Intell.*, vol. 35, no. 6, pp. 1397–1409, Jun. 2013.
- [15] B. Y. Zhang and J. P. Allebach, "Adaptive bilateral filter for sharpness enhancement and noise removal," *IEEE Trans. Image Process.*, vol. 17, no. 5, pp. 664–678, May 2008.
- [16] Z. Li, J. Zheng, Z. Zhu, S. Wu, W. Yao, and S. Rahardja, "Content adaptive bilateral filtering," in *Proc. IEEE Int. Conf. Multimedia Expo*, Jul. 2013, pp. 1–6.
- [17] L. Itti, C. Koch, and E. Niebur, "A model of saliency-based visual attention for rapid scene analysis," *IEEE Trans. Pattern Anal. Mach. Intell.*, vol. 20, no. 11, pp. 1254–1259, Nov. 1998.

- [18] C. C. Pham, S. V. U. Ha, and J. W. Jeon, "Adaptive guided image filtering for sharpness enhancement and noise reduction," in *Advances in Image and Video Technology*. Berlin, Germany: Springer-Verlag, 2012.
- [19] G. Petschnigg, M. Agrawala, H. Hoppe, R. Szeliski, M. Cohen, and K. Toyama, "Digital photography with flash and no-flash image pairs," *ACM Trans. Graph.*, vol. 22, no. 3, pp. 664–672, Aug. 2004.
- [20] E. Eisemann and F. Durand, "Flash photography enhancement via intrinsic relighting," *ACM Trans. Graph.*, vol. 22, no. 3, pp. 673–678, Aug. 2004.
- [21] A. Zomet and S. Peleg, "Multi-sensor super-resolution," in *Proc. 6th IEEE Workshop Appl. Comput. Vis.*, Dec. 2002, pp. 27–31.
- [22] A. Torralba and W. T. Freeman, "Properties and applications of shape recipes," in *Proc. IEEE Comput. Vis. Pattern Recognit.*, Jun. 2003, pp. 383–390.
- [23] A. Levin, D. Lischinski, and Y. Weiss, "A closed-form solution to natural image matting," *IEEE Trans. Pattern Anal. Mach. Intell.*, vol. 30, no. 2, pp. 228–242, Feb. 2008.
- [24] R. C. Gonzalez and R. E. Woods, *Digital Image Processing*. Upper Saddle River, NJ, USA: Prentice-Hall, 2002.
- [25] A. K. Moorthy and A. C. Bovik, "A two-step framework for constructing blind image quality indices," *IEEE Signal Process. Lett.*, vol. 17, no. 5, pp. 513–516, May 2010.
- [26] S. G. Narasimhan and S. K. Nayar, "Chromatic framework for vision in bad weather," in *Proc. IEEE Conf. Comput. Vis. Pattern Recognit. (CVPR)*, Jun. 2000, pp. 598–605.
- [27] R. T. Tan, "Visibility in bad weather from a single image," in *Proc. IEEE Conf. Comput. Vis. Pattern Recognit. (CVPR)*, Jun. 2008, pp. 1–8.
- [28] X. Lv, W. Chen, and I-F. Shen, "Real-time dehazing for image and video," in *Proc. 18th Pacific Conf. Comput. Graph. Appl.*, Sep. 2010, pp. 62–69.
- [29] J. Pang, O. C. Au, and Z. Guo, "Improved single image dehazing using guided filter," in *Proc. APSIPA ASC*, Xi'an, China, 2011, pp. 1–4.
- [30] M. van Herk, "A fast algorithm for local minimum and maximum filters on rectangular and octagonal kernels," *Pattern Recognit. Lett.*, vol. 13, no. 7, pp. 517–521, Jul. 1992.
- [31] E. B. Goldstein, *Sensation and Perception*. Wadsworth, OH, USA: Cengage Learning, 1980.
- [32] A. J. Preetham, P. Shirley, and B. Smits, "A practical analytic model for daylight," in *Proc. SIGGRAPH*, 1999, pp. 91–100.